



Evaluating the combustion and flame extension characteristics of cable fire in utility tunnels with spontaneous combustion scenarios: An experimental study

Desheng Xu^a, Yanfeng Li^{a,*}, Jiaxin Li^a, Hua Zhong^{b,*}, Junmei Li^a, Dengkai Tu^a, Youbo Huang^c

^a Beijing Key Laboratory of Green Built Environment and Energy Efficient Technology, Beijing University of Technology, Beijing, China

^b School of Architecture, Design and Built Environment, Nottingham Trent University, Nottingham NG1 4FQ, United Kingdom

^c College of Safety Engineering, Chongqing University of Science and Technology, Chongqing, China

ARTICLE INFO

Keywords:

Utility tunnel
Cable fire
Combustion characteristics
Flame height
Spread rate

ABSTRACT

A cable fire in a utility tunnel can cause severe damage to the electric power supply in cities. This study aims to understand the combustion and flame spread characteristics of cable fires, which are mainly caused by overheating from the excessive current at the interconnections of the cables under spontaneous combustion. Fire experiments were conducted in a 1:6 scale model of a utility tunnel to analyse the flame spread characteristics under different heat release rates (HRRs), vertical distances, and transverse distances. The findings of this study show that the total burning time of the cable fire increases as the cable diameter increases, and the HRR also shows an increasing trend. Additionally, the spatial location of the cable fire has a significant impact on the flame spread. The terms H_c^* and D_c^* are defined to characterize the flame height and a general prediction model of the dimensionless flame height influenced by cable spontaneous combustion is proposed. A dimensionless model is also established to describe the flame spread rate. This research provides valuable guidance to aid in the development of fire safety measures in utility tunnels.

1. Introduction

As global urbanisation accelerates, urban space is increasingly stretched. The utility tunnel is an intensive underground infrastructure that concentrates electric power, telecommunication, gas, and other engineering pipelines in the same underground space (Ye et al., 2021). It plays a significant role in easing the strong demand for land resources and increasing socio-economic benefit, urban utility tunnels have been widely chosen as a key technology to address the construction of urban lifeline systems in many countries (Pan et al., 2020; Huang et al., 2022). For example, up to 2020, the total mileage of utility tunnels in China has reached more than 5000 km, with 500 cities covered (Wang et al., 2018). However, with the fierce development of urban utility tunnels, the fire problem has become increasingly prominent. The power cabins are a major compartment in utility tunnels with a high risk of fire accidents. According to the investigation, the fire is likely to occur at the

cable joints due to poor connections, such as cable short circuits, cable ageing and current overload (Bai et al., 2020). In October 2015, a 10-hour-long cable fire burnt in Seoul (Korea), which caused great damage. Therefore, it must investigate the combustion and flame characteristics of cable fire scenarios to reveal the fire hazards in the utility tunnels.

The combustion characteristics of cable have been widely studied in surface temperature, time of ignition (T_i), heat release rate (HRR) and mass loss rate (MLR). The Factory Mutual Research Corporation and the European Commission were the first to conduct detailed tests on the combustion characteristics of utility tunnel cables (Klein et al., 1997; Grayson et al., 2000). They found that the arrangement of the cables could largely influence the experimental results, with the cables burning most vigorously when placed vertically. Bertrand et al. (2002) studied the fire resistance characteristics of cables through a series of test experiments and proposed a calculation method and evaluation criteria for cable failure. Some burning experiments (Martinka et al., 2018) were

* Corresponding authors at: Beijing University of Technology, Beijing 100124, China (Y. Li). Nottingham Trent University, Nottingham NG1 4FQ, United Kingdom (H. Zhong).

E-mail addresses: liyanfeng@bjut.edu.cn (Y. Li), hua.zhong@ntu.ac.uk (H. Zhong).

¹ Address: Beijing University of Technology, Beijing 100124, China.

<https://doi.org/10.1016/j.tust.2023.105244>

Received 13 February 2023; Received in revised form 21 April 2023; Accepted 4 June 2023

Available online 16 June 2023

0886-7798/Crown Copyright © 2023 Published by Elsevier Ltd.

This is an open access article under the CC BY-NC-ND license

(<http://creativecommons.org/licenses/by-nc-nd/4.0/>).

Nomenclature	
Q	heat release rate (kW)
Q^*	dimensionless heat release rate
H_t	tunnel ceiling height (cm)
H_c	height between the cable and tunnel floors (cm)
H_f	flame height beneath the ceiling (cm)
g	gravitational acceleration (m/s^2)
M_{O_2}	the initial mass flow rate of oxygen (kg/s)
$M^*_{O_2}$	the mass flow rate of oxygen during combustion (kg/s)
M	the mass loss rate of the steady-state combustion phase (g/s)
H_c^*	dimensionless cable height
D_c	distance between the cable and tunnel side wall (cm)
D	tunnel width (cm)
D_c^*	Dimensionless transverse distance
V_f^*	Dimensionless flame spread rate
V_f	flame spread velocity (cm/s)
A_f	flame area (cm^2)
V_c^*	dimensionless critical velocity
E	oxygen-consuming heat of the material (MJ/kg)
ΔH_c	the heat of combustion of the fuel (MJ/kg)
X_{O_2}	the initial molar fraction of oxygen
$X^*_{O_2}$	the molar fraction of oxygen measured during the experiment
C_e	orifice coefficient ($kg^{1/2}m^{1/2}k^{1/2}$)
ΔP	pressure through the orifice flowmeter (Pa)
T_e	smoke temperature (K)
m_e	the mass flow rate of the outflow smoke (kg/s)
EHC	average effective heat of combustion (kJ/g)
HRR	heat release rate (kW)
MLR	mass loss rate (g/s)
$pHRR_0$	first peak heat release rate (kW)
$pHRR_1$	highest heat release rate (kW)
t_{HRR}	time after ignition to the highest heat release rate (s)
T_t	total burning time (s)
c_p	the specific heat capacity of air (kJ/(kg·K))
r	the ratio of the oxygen to the fuel
<i>Greek letters</i>	
ρ_∞	ambient density (kg/m^3)
α	volume expansion factor
β	volume change of the gas
<i>Subscripts and subscripts</i>	
*	dimensionless expression
f	flame characteristic
c	cable position

conducted using a cone calorimeter to investigate the influence of the distance between cables and the material of the cable supports on fire characteristics. Results showed that the HRR of the cable fire increases as the distance increases and the value of thermal conductivity decreases. Based on the use of a flame detection algorithm, some cable fire experiments were conducted by [Beji et al. \(2016\)](#). Results show that the VFA (video fire analysis) technique can provide a good reconstruction of the HRR profile from the temporal change of the fire and flame at horizontally arranged trays. A series of fire spread tests ([Zavaleta and Hanouzet, 2019](#)) on horizontal trapezoidal cable trays were studied, and the FLASH-CAT model was improved by utilising video fire analysis methods to achieve high prediction accuracy. [Tao et al. \(2019\)](#) studied the cable burning characteristics by some cone calorimeter tests and full-scale experiments, and a calculation model was proposed to predict the HRR of the transverse vertical cable fire.

Based on previous studies ([Zhang et al., 2017, 2021a](#)), the fire flame is formed by the mixture of unburnt fuel and air entrainment during the diffusion process. Numerous experimental studies of flame extension in tunnels have been widely conducted, and many valuable models have also been proposed ([Gao et al., 2017; Tang et al., 2021; Zhang et al., 2021b; Zhou et al., 2020](#)). Some important parameters such as the HRR of the fire source, the fire location and the dimensions of the tunnel have been considered in the models of the flame extension length. Furthermore, a series of studies have been conducted to investigate the flame characteristics in urban utility tunnels. [Tewarson and Khan \(1989\)](#) conducted an experimental study of flame spread in a vertical cable tray and the influence mechanisms of cable materials, dimensions and other parameters on fire propagation were analyzed. A prediction formula for the rate of fire propagation was proposed, and the fundamental conditions for the cable fire allowed to spread were also given. Based on the fire experiments ([Delichatsios and Delichatsios, 1994](#)), some key parameters of cable fire such as ignition time and combustion characteristics were summarised. Taking them into consideration, a cable fire spread prediction formula applicable subject to open space conditions was also proposed. Some large-scale fire tests ([Passalacqua et al., 2013](#)) were conducted on power cables in both the horizontal and vertical directions. The results indicate that flame propagation is fast in vertical cable trays, while fire is quickly extinguished in horizontal tests once the

ignition source is removed. A flame spread model ([Huang et al., 2019](#)) of vertical cable fire subject to confined and open spaces was established. And in terms of thermal characteristics, a vertical cable tray fire was divided into three zones. [An et al. \(2020\)](#) experimentally investigated the influences of cable vertical distance and horizontal spacing on the flame characteristics in a utility tunnel. Based on the experiment phenomenon of multilayer cables, they found that the extreme distance that the cable fire could spread to the upper layer is 10.0 cm, and the rate of flame spread reached a peak value at the vertical distance of 7.5 cm and the spacing is 2.5 cm. [Pan et al. \(2022\)](#) analyzed the relationship between the upper extension flame and the curved ceiling through experiments in two kinds of utility tunnels. A prediction model of the flame extension lengths beneath the curved ceiling was proposed, considering the factors of HRR, fire source size and utility tunnel geometry.

In summary, the understanding of cable fire in utility tunnels is crucial for ensuring the safety of power supply in cities. Previous studies have contributed to this understanding, however they have certain limitations. (1) most cable fire studies have focused on continuous ignition caused by oil pool fire or radiant heating, which do not accurately reflect cable spontaneous combustion. (2) oil pool fire is used as the fire source in utility tunnel fire experiments, making it difficult to simulate cable fire scenarios. Moreover, the excessive current can result in local overheating of the cable, leading to cable self-combustion. While studies on cable fire characteristics in self-ignition (spontaneous combustion) scenarios are limited. Additionally, the spatial location of the cable also has an important impact on the development of the fire ([Poreh et al., 2020](#)). And the impact of cable ignition from joint point and flame spreading along the cable has not been fully explored.

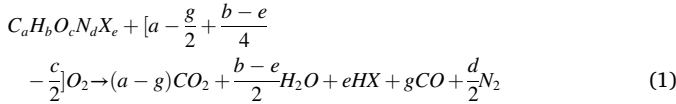
To address these limitations, this study aims to enrich our understanding of cable fire in utility tunnels by combining experimental and theoretical approaches. Through cable-burning tests, the fire resistance performance of cables was studied to understand cable combustion characteristics, such as the combustion phenomenon, burning time, HRR and MLR. Then, a series of cable fire experiments were conducted in a 1:6 scale model of a utility tunnel to analyse flame spread characteristics under different HRRs, cable vertical and transverse distances. The results of this study provide valuable insights into the flame spread characteristics of cable fires and prediction models were proposed to

estimate flame height and flame spread rate in cable self-ignition scenarios. This study is expected to provide effective guidance for the safety monitoring of utility tunnels in different cable fire scenarios.

2. Theoretical analysis

2.1. Heat release rate (HRR)

The HRR of cable fire is a crucial element in fire safety surveillance, which provides a direct indication of fire risk (Babrauskas and Peacock, 1992). To study the combustion characteristics of cables more clearly, the basic chemical reaction describes the combustion reactions of polymer types such as power cables.



where C , H , O , N , and X are representations of carbon, hydrogen, oxygen, nitrogen, and halogen, respectively; a , b , c , d , and e denote the corresponding atomic numbers.

The amount of heat produced for each unit mass of oxygen during the combustion of a material is approximately equal (Babrauskas, 1984; Hermouet et al., 2021). Therefore, the HRR can be estimated by the oxygen-consuming of a material during the combustion process (Chow and Han, 2011).

$$Q = E(M_{O_2} - M_{O_2}^*) \quad (2)$$

where Q is the heat release rate of the material; M_{O_2} is the mass flow rate of oxygen in ambient environment; $M_{O_2}^*$ is the mass flow rate of oxygen during combustion; E is the oxygen-consuming heat of the material under combustion, and it can be described as follows:

$$E = \frac{\Delta H_c}{r} \quad (3)$$

where ΔH_c is the heat of combustion of the fuel; r is the ratio of the amount of oxygen to the fuel in the complete combustion reaction.

Based on the assumption that the ideal air contains only oxygen and nitrogen and that all combustion gases can be considered incompressible, Eq. (2) can be described as Eq. (4) (Janssens, 1991).

$$Q = E(m_e \frac{M_{O_2}}{M_a}) \cdot (\frac{X_{O_2}^* - X_{O_2}}{\alpha - \beta X_{O_2}}) \quad (4)$$

where m_e is the mass flow rate of the outflow gas; M_a is the molar mass of air; $X_{O_2}^*$ is the molar fraction of oxygen measured in ambient environment; X_{O_2} is the molar fraction of oxygen measured during the experiment; α is the volume expansion factor:

$$\alpha = X_{N_2}^0 + X_{H_2O}^0 + X_{CO_2}^0 + \beta X_{O_2} = 1 + (\beta - 1) X_{O_2} \quad (5)$$

β shows the volume change of the gas phase before and after the reaction:

$$\beta = \frac{a - g + \frac{b-e}{2} + e + d + \frac{g}{2}}{a - \frac{g}{2} + \frac{b-e}{4} - \frac{c}{2}} \quad (6)$$

And the m_e can be calculated as follows:

$$m_e = C_e \sqrt{\Delta P / T_e} \quad (7)$$

where C_e is the orifice coefficient; ΔP is the pressure drop generated by the gas passing through the orifice flowmeter, Pa; T_e is the gas temperature measured at the orifice flowmeter.

Substituting Eq. (5), Eq. (6) and Eq. (7) in Eq. (4), the expression of the HRR of the cable under the fire condition is obtained:

$$Q = \frac{\Delta H_c}{r} \cdot (C_e \sqrt{\Delta P / T_e} \cdot \frac{M_{O_2}}{M_a}) \cdot (\frac{X_{O_2}^* - X_{O_2}}{\alpha - \beta X_{O_2}}) \quad (8)$$

2.2. Flame extension

In tunnel fires, when the produced flame is lower than the ceiling, the flame height H_f can quantify non-dimensionally against HRRs and well collapsed by a 2/5 power law function (Zhang et al., 2014):

$$H_f / R = 4.55 Q'^{2/5} \quad (9)$$

where R is the diameter of the fire source; Q' is the non-dimensional HRR of the fire source, defined as the following:

$$Q' = \frac{Q}{\rho_\infty T_\infty c_p g^{1/2} R^{5/2}} \quad (10)$$

where Q is the HRR of the source; ρ_∞ is the ambient air density; T_∞ is the ambient air temperature; c_p is the specific heat of air at constant pressure; g is the gravitational acceleration.

With the limitations of the side wall and ceiling to flame extension length, the following correlation was summarised as follows (Tao et al., 2017):

$$\frac{L_f}{H} = C \cdot Q_{BH}^{*2/5} \quad (11)$$

$$Q_{BH}^* = \frac{Q}{\rho_\infty T_\infty c_p g^{1/2} B H_f^3} \quad (12)$$

where L_f is the flame length; B is the length of the rectangular edge parallel to the wall; H_f is the tunnel height.

Thus, for the special space position of the cable fire in a utility tunnel, the dimensional analysis expression of flame extension height is as follows:

$$H_f \sim f(H_t, D, H_c, D_c, Q) \quad (13)$$

where H_f is the flame height beneath the ceiling; D is the tunnel width; H_c is the vertical distance between the cable and floor; D_c is the transverse distance between the cable and side wall.

3. Experimental setups

3.1. Experimental cables

Cables are the main combustible material in utility tunnels. And it is also a major cause of fire accidents (Klauck et al., 2022). Although most of the cables used in the utility tunnels are flame-retardant, large-scale fire spread can still occur in the event of strong electrical currents (Meinier et al., 2018). Considering safety requirements, fire experiments are not conducted using flame-retardant cables under electrical condition in this work. And the use of cables that are not highly flame-retardant can reflect the spread of cable fires in current-free conditions. Through investigation, YZ cable is used in this work to investigate the fire combustion and flame extension characteristics in fire scenarios (An et al., 2020). It is commonly called heavy-duty general-purpose rubber cable and it applies to power tools and various mobile electrical equipment. The YZ cable is not highly flame-retardant and an actual image of the material properties of the cable is shown in Fig. 1. The cables tested in this paper contain various numbers of cores, from two to four, which are made of oxygen-free copper. The material of the cable outer sheath and core-sheath is neoprene, which is a kind of natural polymer mainly compound with *cis*-1-4 polyisoprene, and the molecular formula is $(C_5H_8)_n$. The insulation layer material is polyvinyl chloride (PVC) and the internal padding material is made up of hemp rope. Details of the physical properties of the cable compounds are given in Table 1.

3.2. Cable burning experiments

To investigate the combustion characteristics of cable fire under

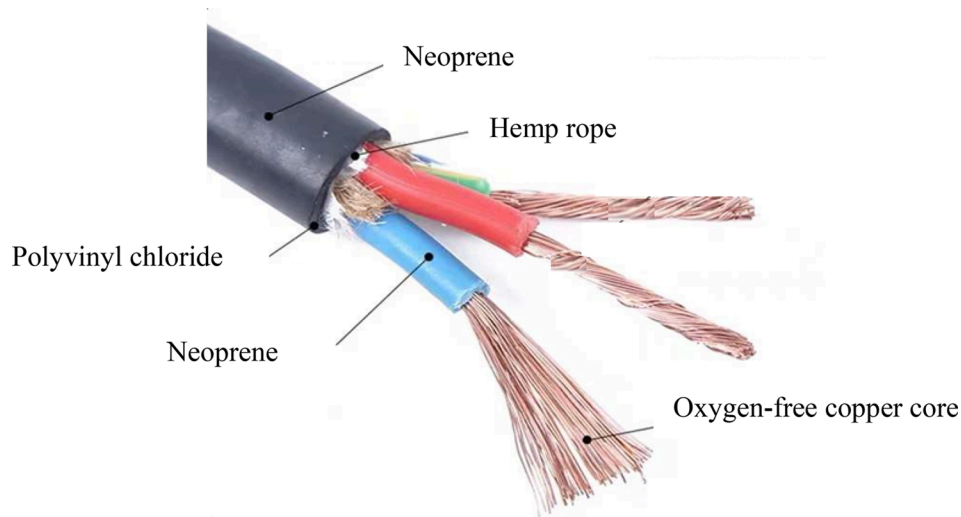


Fig. 1. Diagram of the composition of the experimental cable.

Table 1
The physical properties of cable compounds.

Part	Material	Density (kg/cm ³)	Thermal conductivity (W/(m·K))	Specific heat capacity(kJ/(kg·K))
Core	Oxygen-free copper	387.0	8.94	0.38
Sheath	Neoprene	1.25	0.19	1.70
Insulation layer	Polyvinyl chloride	1.50	0.20	1.50
Internal padding	Hemp rope	0.80	0.06	1.51

spontaneous combustion status, such as burning time, HRR, MLR, etc. a series of burning tests are conducted by the cable-burning experimental platform. Some improvements are made based on the cone calorimeter (Standard, 1993), and Fig. 2 shows the schematic of the combustion platform and measurement apparatus.

The smoke trap is a 1.5-m × 1.5-m space enclosed by four angled steel plates. The distance between the bottom of the four-angle steel plates and the highest level of the cable tray is 5.0 cm. It ensures that the cable samples are in sufficient oxygen for combustion. The cable trays are made of stainless steel and consist of five layers with a spacing of 5.0 cm. To facilitate the experiments, the cable trays are designed to be portable to make it easier to place and remove cables in experiments. An electronic scale is positioned directly below the bottom of the cable tray to record the mass change of the cable during combustion. The measurement range was 0–1.0 kg with a minimum accuracy of 0.001 g. The

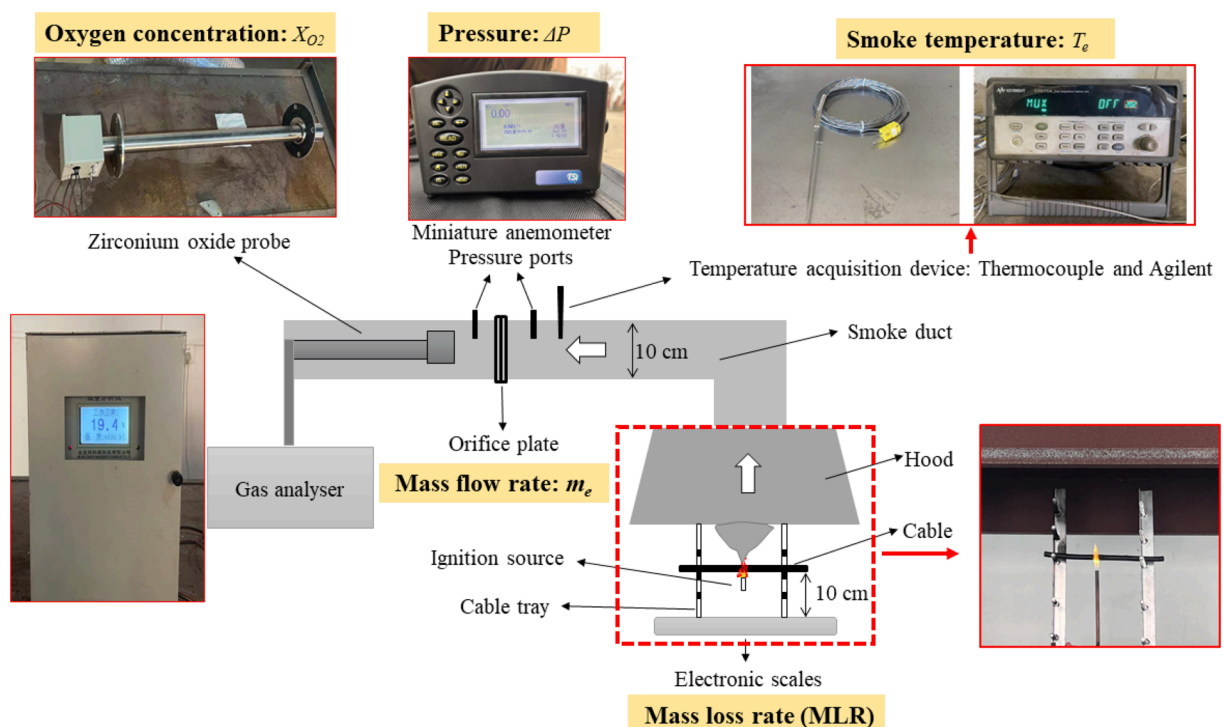


Fig. 2. Layout and diagram of the combustion platform.

zirconium oxide probe is used in the smoke duct to measure the oxygen concentration in the air. And the value of the oxygen concentration is displayed in a gas analyser and stored in PC. Its accuracy could reach 0.001 %. Two differential pressure ports are fixed in the smoke duct (diameter is 10 cm) to measure the differential pressure flowing through the orifice plate (diameter is 5 cm). The instrument is a TSI high-precision miniature anemometer DP-CALC 8715 with a range of ± 100.00 Pa with an accuracy of ± 2 %. The temperature acquisition device is composed of K-type thermocouples and an Agilent 34970A. The measurement range is $0\text{ }^{\circ}\text{C} \sim 1300\text{ }^{\circ}\text{C}$ with an accuracy of ± 0.1 % (Standard, 1994).

To test the fire properties of cables, six different sizes of YZ copper core rubber cables are selected in the cable-burning tests. The details of combustion test conditions are listed in Table 2. As shown in Fig. 2, a 15.0 cm length of cable is placed on the cable tray at a height of 10.0 cm above the floor during the combustion tests. The igniter is placed 5.0 cm beneath the cable and controlled by liquefied petroleum gas with a fixed HRR of 0.1 kW. Once the fire has ignited the cable for 5 s, the ignition source is immediately switched off to achieve spontaneous combustion. The environmental conditions of the tests are as follows: atmospheric pressure is 100.71 kPa, oxygen concentration is 20.4 %, ambient temperature is $10\text{ }^{\circ}\text{C}$, and humidity is 60 %.

3.3. Utility fire experiments

To investigate the behavioural mechanisms of flame extension in a utility fire, a 1:6 small-scale utility tunnel is built using the Froude scaling method. Fig. 3 shows the outline of the experimental platform and a diagram. The dimensions of the utility are 6.0 m long, 0.4 m wide, and 0.5 m high, representing the full-scale utility is 36 m long, 2.4 m wide, and 3.0 m high. The experimental platform is divided into three sections and connected by bolts. There are five layers of cable tray in the middle section and the lowest layer is 10.0 cm from the ground. The layer spacing is 5.0 cm high and the width of each cable tray is 10.0 cm. The platform is also equipped with air inlets and exhausts with switchable seals (which can be opened and closed) at both ends. In order to closely match the real environment of the fire scenario in the utility tunnel, the air inlets and exhausts are entirely enclosed during the experiment. Both the inner wall and the top ceiling are made of three layers of material. The outer layer is made of a thick steel sheet (1.5-cm

cold chilled steel) and the inner layer is made of fireproof board. The external wall surface is installed with 1.0-cm thick toughened fireproof glass, which can resist high temperatures around $1000\text{ }^{\circ}\text{C}$. A Sony HDR-CX450 digital camera with a 4.3 mm sensor size and 2.2 megapixels (25 fps) is used to record the development of the cable fire. The camera is positioned opposite the glass of the experimental platform to obtain the flame video of utility fire for further analysis of flame spread characteristics.

The cables with six different diameters, which have been tested in cable-burning experiments, are selected as the fire source to perform flame spread characteristics in the utility fire experiments. The range of the HRRs corresponding to these cables is between 0.36 kW and 0.46 kW. The details of the utility fire experiments are described in Table 3. One cable with a length of 15.0 cm is used for each fire scenario and placed on one cable tray, the arrangement is given in Fig. 3 (a). The height of the cable from the ground H_c and the transverse distance from the side wall D_c as well as the diameter of the cable are changed. The ignition source is controlled by liquefied petroleum gas with a fixed HRR of 0.1 kW and placed 5.0 cm under the cable. Once the cable has been lit for 5 s, the valve of the ignition source is immediately switched off to achieve a cable fire under spontaneous scenario.

3.4. Data processing methods

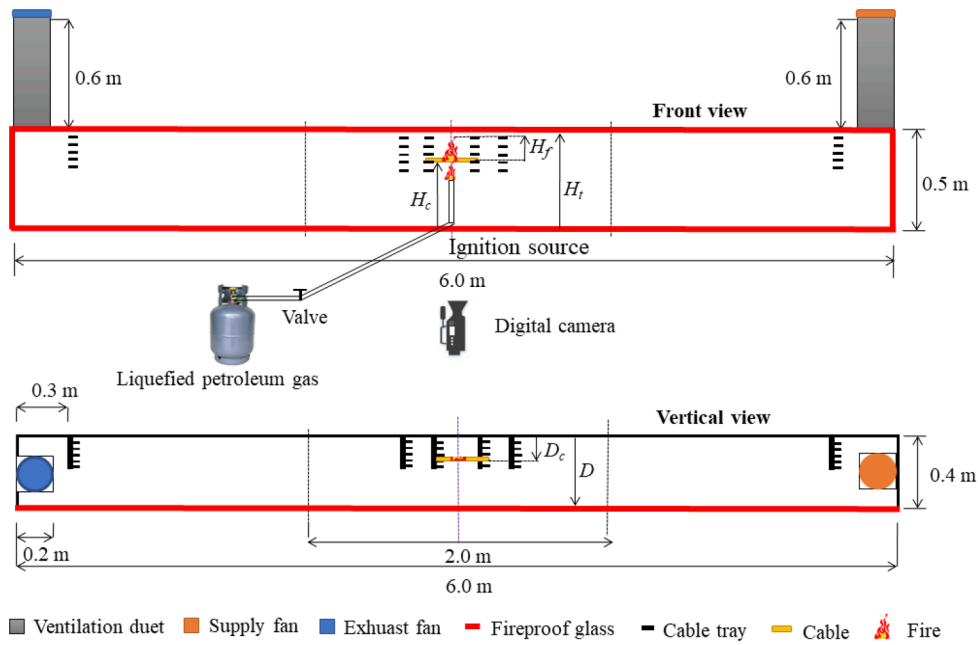
The flame characteristics of cable fires are important indicators of the hazard level. Visual inspection (Li et al., 2023), sensor-assisted measurement (Vandecasteele et al., 2016) and image processing (Hu et al., 2013) are common methods currently used to obtain flame patterns. Among them, the approach of image processing is the most time-consuming but highly accurate. It not only guarantees fine-grained processing of the flame video, but also gives the probability distribution of flame occurrence to express the flame characteristics. In this work, image processing based on the Otsu method (Blevins and Pitts, 1999; Otsu et al., 2007) is adopted to get fire flame data. It is also the most commonly used method in related research that enables the test data to be sufficiently intuitive and accurate. The detail steps of the processing are as follows and shown in Fig. 4. (1) segmenting the captured flame video and intercepting it into multiple sub-videos according to the 10-s interval. (2) processing each sub-video segment using MATLAB software programming to decompose the flame images every

Table 2
Cable combustion test conditions.

Condition number	Cross-section	Number of cores	Diameter(cm)	T_i (s)	ΔP (Pa)	T_e (K)	m_e (kg/s)	$pHRR_0$ (kW)	$pHRR_1$ (kW)	MLR (g/s)
A1		2	0.85	315	2.12	365.2	2.08	0.186	0.362	0.034
A2		2	0.93	325	2.23	369.6	2.15	0.203	0.387	0.036
A3		2	1.00	330	2.31	374.7	2.20	0.216	0.409	0.039
A4		2	1.12	345	2.45	379.7	2.45	0.239	0.43	0.042
A5		3	1.05	355	2.37	377.3	2.24	0.259	0.445	0.040
A6		4	1.20	365	2.52	382.0	2.63	0.292	0.463	0.044



(a) Actual outline of the 1:6 small-scale utility tunnel.



(b) Schematic diagram of the 1:6 small-scale utility tunnel.

Fig. 3. Actual outline and diagram of the 1:6 small-scale utility tunnel.

Table 3
Summary of experimental scenarios.

Scenario number	HRR (kW)	Vertical distance H_c (cm)	Transverse distance D_c (cm)
B1-B12	0.36	10,20,30	1,4,7,10
B13-B24	0.39	10,20,30	1,4,7,10
B25-B36	0.41	10,20,30	1,4,7,10
B37-B48	0.43	10,20,30	1,4,7,10
B49-B60	0.45	10,20,30	1,4,7,10
B61-B72	0.46	10,20,30	1,4,7,10

20 frames. (3) converting each original image Fig. 4 (a) into a grey-scale image Fig. 4 (b) based on the brightness of each pixel point. And converting the image into a binary grey-scale image Fig. 4 (c) using the Otsu

method. (4) multiple consecutive binary images are subjected to statistical analysis. Averaging of the values of these continuous binary images at each individual pixel position, and a statistical probability graph of the flame appearance is obtained, as shown in Fig. 4 (d). (5) eventually, a two-dimensional profile of the flame occurrence probability distribution (p) is obtained and shown in Fig. 4 (e). The flame height, flame length, and flame area can be derived from the probability of $p = 50\%$ (Hu et al., 2019).

4. Results and discussion

4.1. Combustion characteristics

The entire process of cable combustion can be divided into five stages according to the phenomenon: 1. ignition, 2. single-fire development, 3.

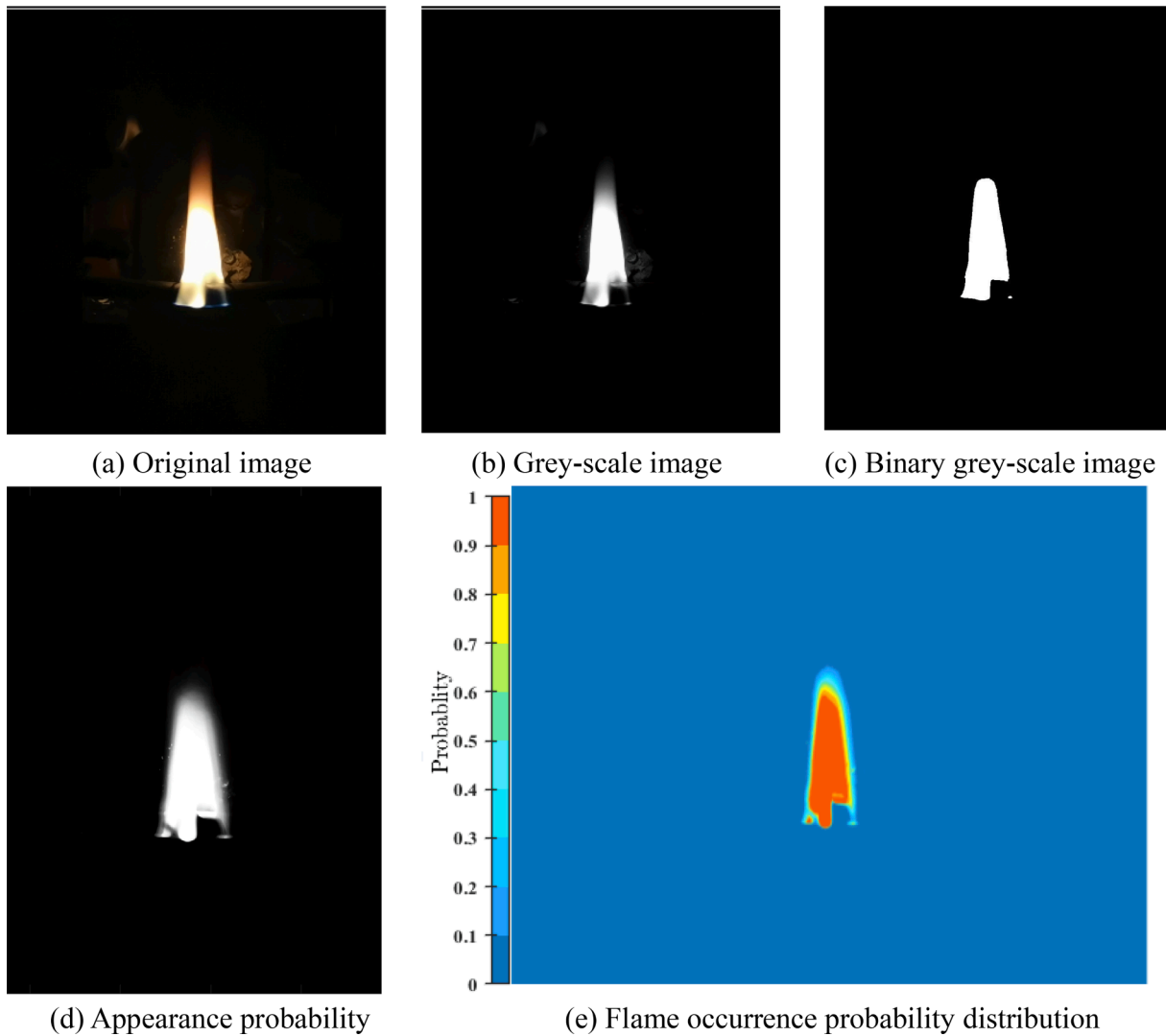


Fig. 4. Flame image processing.

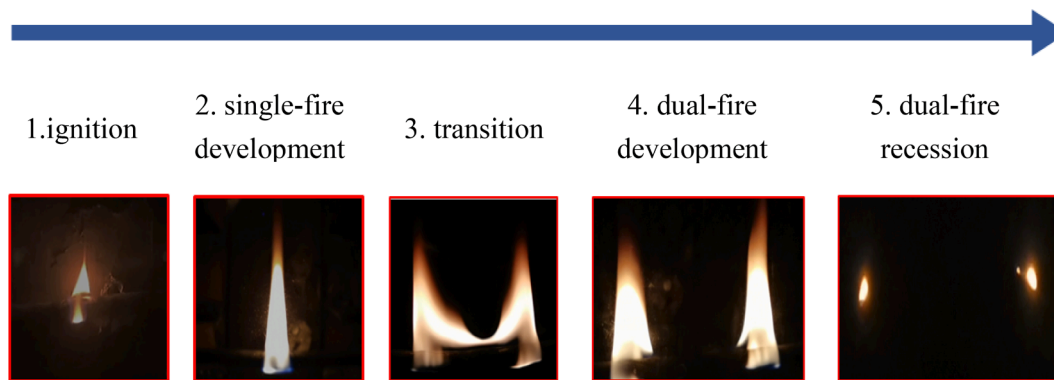


Fig. 5. Different combustion stages during cable burning.

transition, 4. dual-fire development and 5. dual-fire recession, as shown in Fig. 5. It can be found that once the cable is ignited, the flame starts to develop at the bottom of the sheath and evolves to the internal surface and the upper surface. Then, during the single-fire development stage, the fire gradually burns through the entire cable cross-section (Ye et al., 2021). Afterwards, the flame area increases and the upper front of the flame changes from a single top to a double top, which is the transition

stage. As the combustible material at the initial location of the cable fire gradually burns out, the flame is insufficient to maintain the original shape. And the fire ignites the surrounding combustible sheath in a horizontal direction, resulting in a single-fire gradually evolving into a double-fire. Following this, the flame develops into a dual-fire development and gradually burns along the cable towards both ends. Subsequently, in dual-fire recession stage, there is a gradual weakening of



Fig. 6. Diagram of cable combustion product.

the burning level and reduction of the flame until extinguished. The spontaneous combustion product is shown in Fig. 6. The outer sheath of the cable is carbonised after burning. There is a white decomposition in the fully burnt area, while the internal copper core cannot be burnt completely.

Fig. 7 shows the variation in oxygen consumption during combustion for different diameter cables. There is a correspondence between the changes in O_2 content and the combustion stages. For example, in the single-fire development phase of the A6 test, the cable burns with greater intensity and the oxygen consumption shows a gradual increase. While in the dual-fire development stage at around 250 s, the oxygen consumption reaches a maximum value of 0.073 %. As the diameter of the cable increases, oxygen consumption tends to increase. This is mainly due to the increase in the thickness of the cable sheath (Table 2 A1, A2, A3, A4) and the number of copper cores (Table 2 A2, A5, A6). Both of these could contribute to an enlarged amount of combustible material and aggravate the burning of the cable. Additionally, the total burning time T_t of the cable also increases gradually with added diameter. As listed in Table 2, the total burning times are 315 s, 335 s, 330 s, 355 s, 345 s and 365 s, respectively. This suggests that minor changes in cable construction (sheath thickness or the number of copper cores) could delay the burning time. The maximum smoke temperature of the cable under spontaneous combustion scenario is shown in Fig. 8. It can be found that the larger the cable diameter leads to a higher temperature, which also indicates a higher fire hazard.

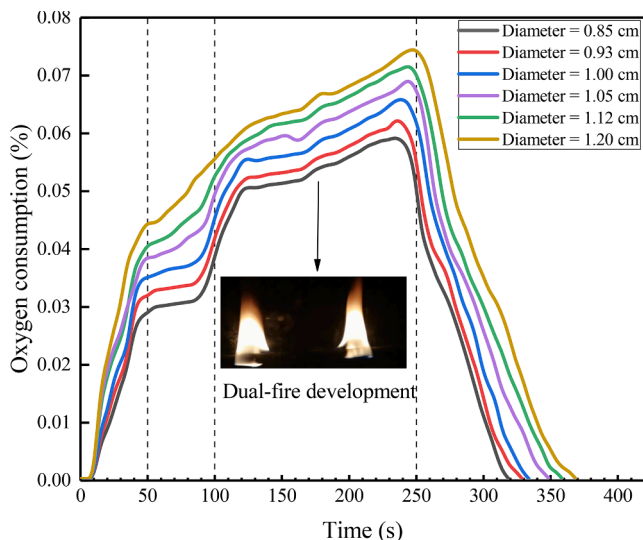


Fig. 7. Oxygen consumption of different diameter cables during combustion.

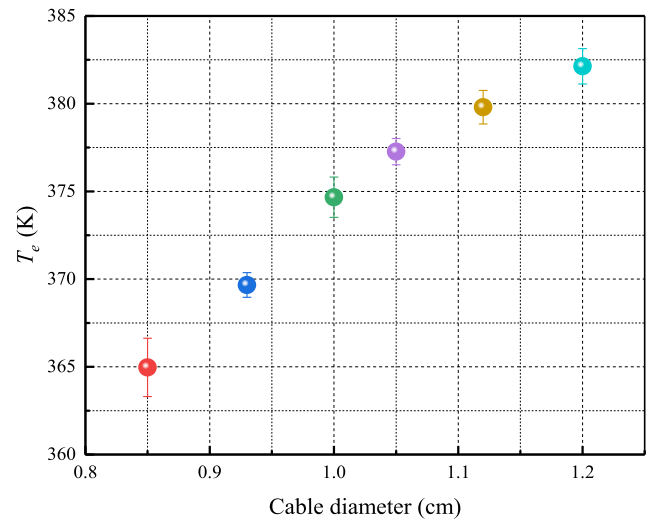


Fig. 8. Maximum smoke temperature of different diameter cables during combustion.

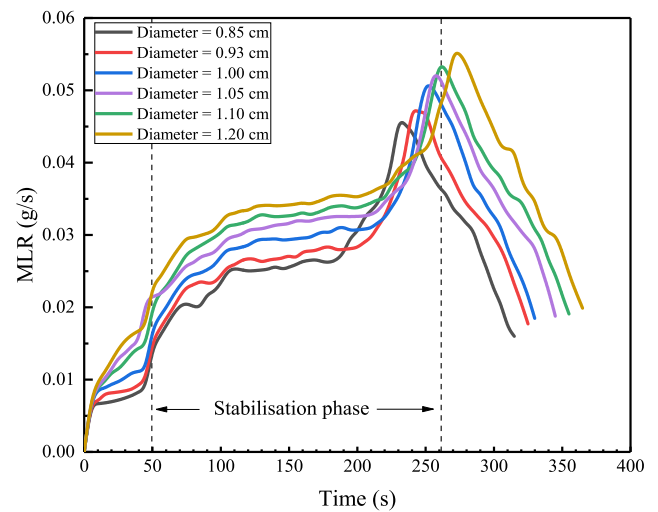


Fig. 9. MLR of different diameter cables during combustion.

As Fig. 9 shows, the MLR increases steadily as the fire develops. And it peaks at the top range at 200 s. Similarly, a greater cable diameter also tends to increase the MLR. Cables with larger diameters also have a longer delay in reaching the peak MLR, and the time difference is up to 35 s at most between tests A1 and A6. The average values of the MLR during the steady-state combustion phase (from 50 s to the reaching the peak MLR) of the cable-burning tests are given in Table 2.

The determination of HRRs for cable fire has attracted a great deal of attention. Two methods are now commonly used to calculate it: oxygen consumption method (Tao et al., 2019) and mass loss method (Huang et al., 2022). Based on the theoretical analysis in section 2.1, the HRR is calculated by the oxygen consumption method. It assumes that the molecular formulas of the main components of cable combustion are constant. Thus, α and β can be calculated according to Eq. (6) and Eq. (7) as 1.06 and 1.29, respectively. The ΔH_c of the cable was determined to be 12.77 MJ/kg. In the experiments, the orifice plate diameter is 50 mm, and the orifice plate coefficient C_e is 0.75. Both ΔP and T_e measured during the stabilisation phase are listed in Table 2.

Fig. 10 shows the variation of the HRR for each test condition, which is calculated according to Eq. (8). It can be seen that among $pHRR_0$, $pHRR_1$ and t_{HRR} show a growing trend as the cable diameter increases. In

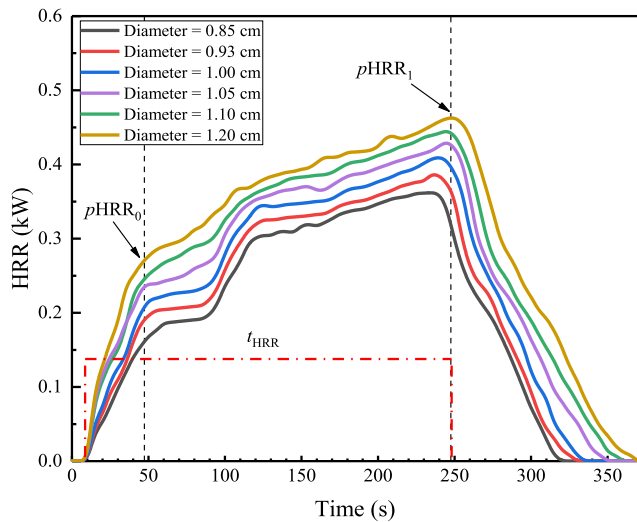


Fig. 10. HRR of different diameter cables during combustion.

particular, by comparing cables with 0.85 cm and 1.20 cm, the $pHRR_1$ is 0.362 kW and 0.463 kW, respectively. With a 41 % increase in cable diameter, the maximum HRR increased by 27.9 %. Additionally, t_{HRR} is also delayed by 15 s. This is a result of the additional combustible material causing the cable to burn more fully and permanently, thus increasing the total burning time. To ensure the accuracy of the HRR calculation in this work, the mass loss method is used for validation, and the formula is given in Eq. (14).

$$Q = EHC \cdot M \tag{14}$$

where EHC is the average effective heat of cable burning, taken as 12.77 kJ/g (Huang et al., 2021); M is the mass loss rate of the steady-state combustion phase of cable fire.

As Fig. 11 shows, the results of the HRR obtained through the two methods are remarkably similar. Both of them show an increasing trend with adding cable diameter, and the maximum error between them is 8.3 %. However, the value of the oxygen consumption calculation model is slightly lower. This is attributed to the small fluctuation range of oxygen consumption during the burning test. While the mass change is constantly accelerated due to the intensity of combustion, and even the appearance of spalling material. It causes a high variation in the MLR of the cable and the HRR value calculated using the mass loss method is also higher. Therefore, the accuracy of the HRR calculation formula

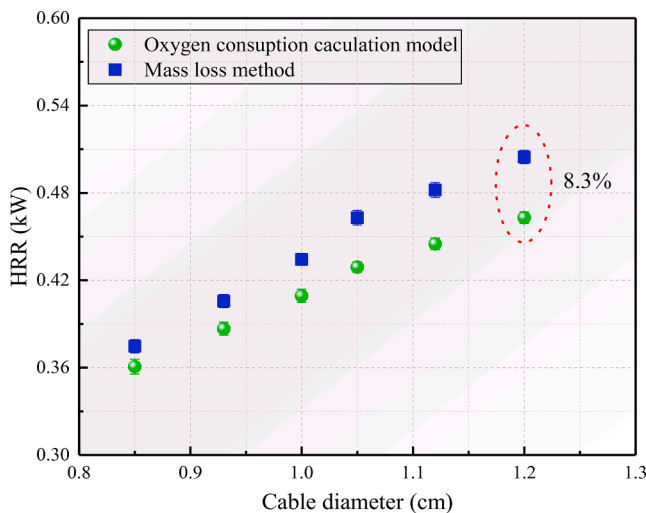


Fig. 11. Comparison of HRR values through two methods.

proposed in this work is reliable, as verified by the above comparison.

4.2. Flame extension characteristics

In order to clearly demonstrate the relationship between flame characteristics and cable HRRs, the MLR changes are recorded in the utility fire experiment. Fig. 12 shows the average values of MLR during the stabilisation phase in cable combustion. By comparison the values of MLR in six burning tests and utility fire experiments, it can be found there are little differences in MLR for cable burning with same diameter in the two test devices. And the relative discrepancy between them is less than 2 %. With the change of cable height and transverse distance, the air entrained by the cable during combustion is lower than that of the open space in cable-burning test. And lower value has occurred in the burning characteristic parameters while the difference can be ignored. According to the discussion in section 4.1, the HRR of the cable under combustion has a same trend as MLR variation. It indicates that the key burning parameters of cable fire in the small-scale utility are almost the same as in the combustion tests. Thus, in the subsequent study, the $pHRR_1$ obtained in the combustion test with six diameter cables are considered as the HRRs of the utility cable fire, as listed in Table 3.

Fig. 13 illustrates the variation in flame height and spread length for a single cable at each combustion stage. As the cable burns into various stages, the flame characteristics change accordingly, such as the flame height H_f and flame area A_f . In Fig. 14, it can be found that the flame height H_f increases rapidly within 50-s ignition. This is due to the buoyancy forces brought about by the fire plume, which drives the flame to expand rapidly in the vertical direction (He et al., 2021). Flame development can be categorized into continuous flame zone and intermittent flame zone (Zhang et al., 2017;Hu et al., 2012). As the combustion enters the transition phase and the dual-fire development phase, the flame height changes in a stable stage and fluctuates within a certain range. And the area of flame fluctuation is the intermittent flame zone. Note that with the increase in HRR of the cable fire, the flame is subjected to stronger buoyancy forces. Resulting in a greater fluctuation of the fire plume in the intermittent flame region. A symmetrical flame extension behaviour is found in the horizontal direction of the cable fire, as shown in Fig. 15. While in the vertical direction, there is a growing trend in flame extension heights H_f and A_f with the increase in HRR. And by comparison with the flame shape of 0.36 kW and 0.46 kW, a 27.9 % increase in fire HRR causes 11.9 % flame height growth and 34.7 % flame area expending.

The dimension of the fire flame area is a significant parameter, which directly reflects the risk of fire. Fig. 16 shows the variation in the flame

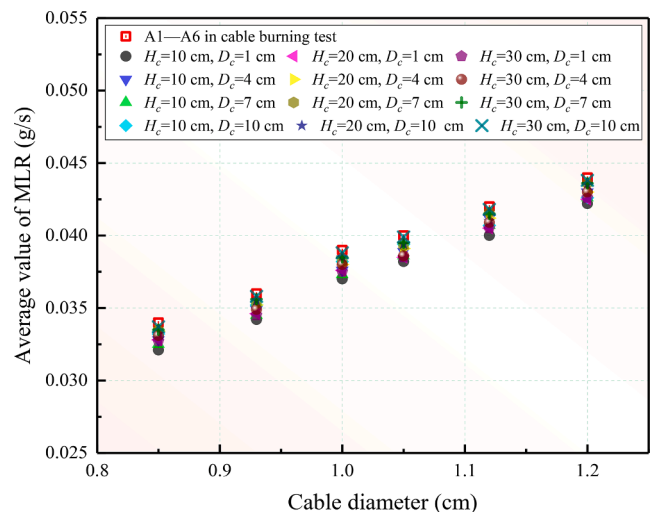


Fig. 12. Comparison of MLR with different diameter cables in burning tests and small-scale utility fire experiments.

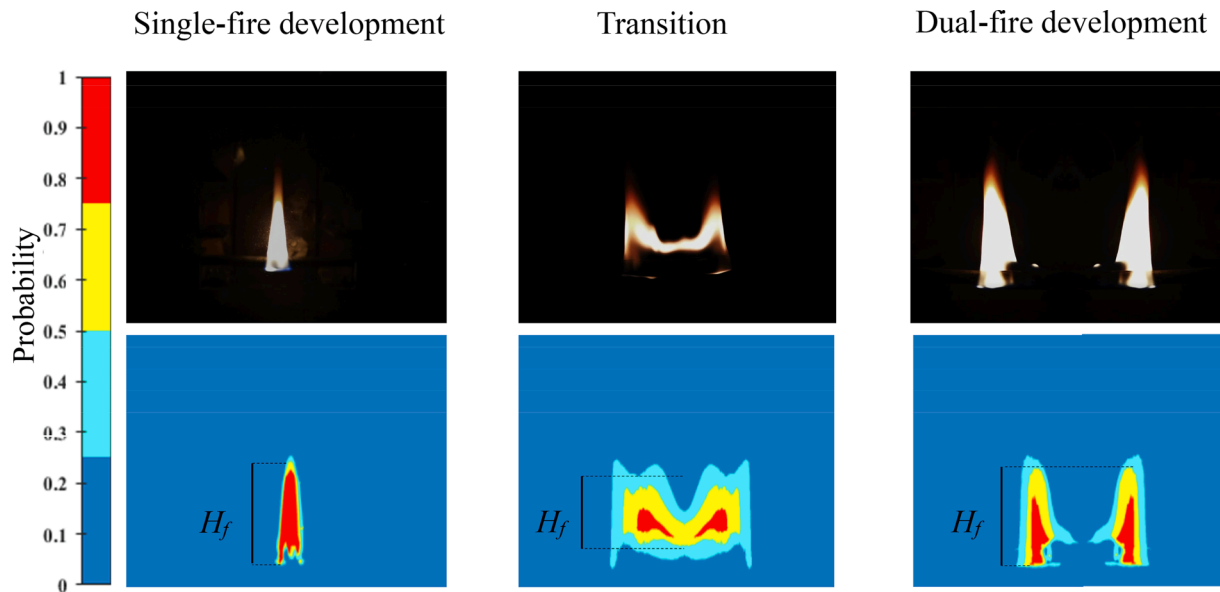


Fig. 13. Flame image processing at each combustion stage.

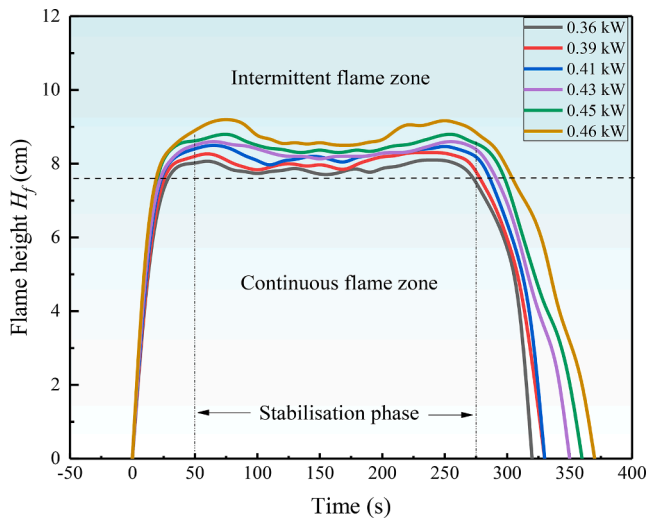


Fig. 14. Flame height variation under different HRRs.

area versus HRR and vertical height of the cable fire at a transverse distance of 10 cm. It can be found that the higher the cable, the more air the fire entrainment during the combustion development, which also leads to the enlargement of the flame area. Fig. 17 presents the variation in flame height with transverse distance and vertical height for an HRR of 0.46 kW. When the transverse distance is increased, there is a noticeable growth in the flame height of the cable fire plume. Furthermore, the flame height also tends to be greater as the vertical height increases. Fan et al. (2013) have pointed out that the greater the air entrainment, the more rapidly the fire develops, and the flame height increases. When cables are burning, the degree of air entrainment is also affected when the vertical height of the fire as well as the transverse distance changes.

To provide a clear description of the flame height of cable fires, the dimensionless H_f^* is used to characterize the ratio of the flame height to the height of the cable tunnel, defined as the following:

$$H_f^* = \frac{H_f}{H_t} \tag{15}$$

And Q^* is the non-dimensional heat release rate of cable fire, defined as the following:

$$Q^* = \frac{Q}{\rho_\infty T_\infty c_p g^{1/2} H_t^{5/2}} \tag{16}$$

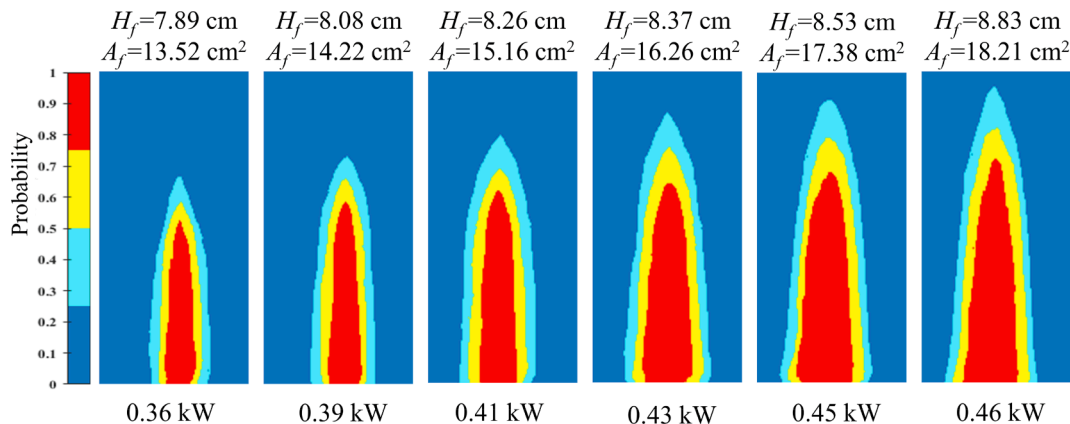


Fig. 15. Flame extension image for cables of different HRRs.

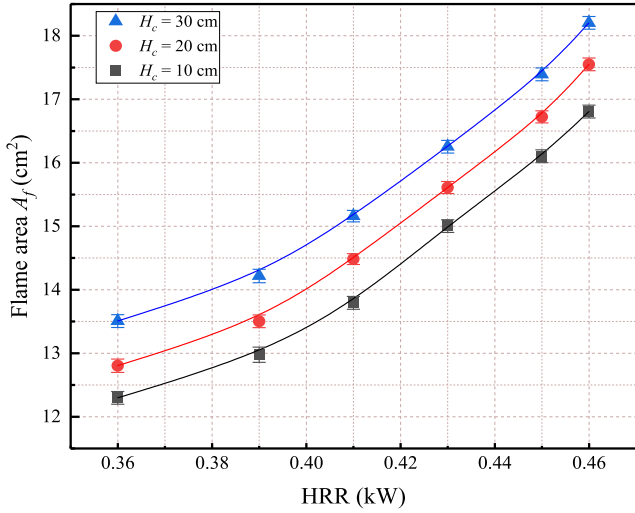


Fig. 16. Flame area with HRRs and vertical height at a transverse distance of 10 cm.

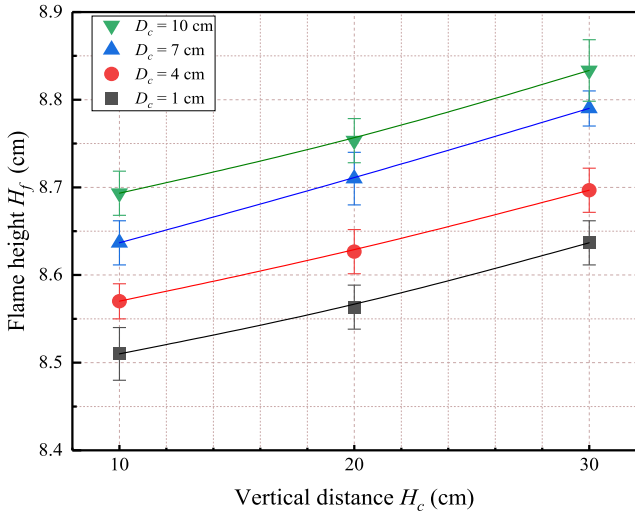


Fig. 17. Flame height with transverse distance and vertical height under 0.46 kW.

Fig. 18 shows the relationship between the dimensionless flame extension height and HRR inside the utility tunnel under spontaneous combustion. The experimental data in this paper also presents well proportional relationship between them. However, as the transverse distance between the burning cable and the side wall decreases, the values of Zhang’s model (Zhang et al., 2014) are greater than the experimental data. This is mainly attributed to the fact that the decreasing lateral distance inhibits the development of the fire as well as the flame height. In Tao’s model (Tao et al., 2017), the distance of the fire source parallel to the side wall is incorporated into the effect on the fire flame. While the parallel length is larger than the distance from the transverse sidewall, resulting in a small prediction value. This suggests that the cable height and transverse distance of the cable fire location should be further included in detail to develop a more general correlation.

Based on the analysis of Eq. (9) and Eq. (11), the flame height is quantified non-dimensionally against HRRs and is well collapsed by a 2/5 power law function. Thus, a new formula for the flame height can be derived as follows:

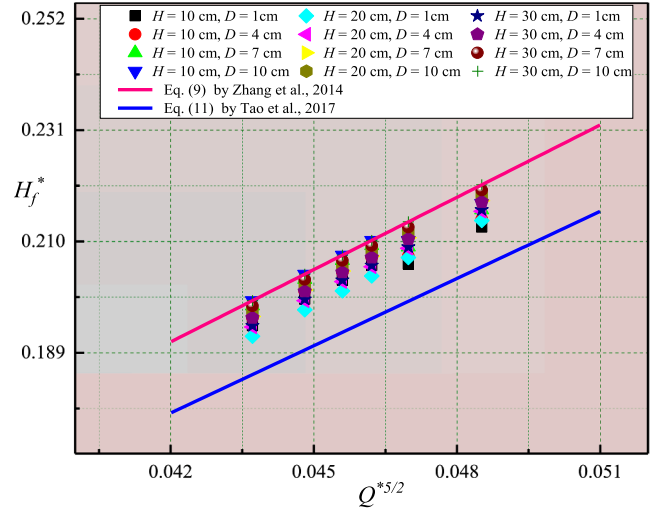


Fig. 18. Comparison of the experimental measured results with the proposed empirical model.

$$H_f^* = \frac{H_f}{H_i} \sim \gamma \cdot Q^{*5/2} \quad (17)$$

where γ is a constant number, and it can be expressed as follows:

$$\gamma \sim f(D_c, H_c) \quad (18)$$

Taking into account the effect of sidewall and ceiling on air entrainment of cable fire, as well as the heat transfer mechanism between the smoke and the inner wall and ceiling, the dimensionless H_c^* and D_c^* are introduced to depict the impact on fire (Guo et al., 2020; Gao et al. 2019). H_c^* is the non-dimensional cable vertical height, which reflects the relative height of the cable in the vertical direction of the utility tunnel. And D_c^* is non-dimensional cable transverse distance, which reflects the relative distance of the cable in the transverse direction of the utility tunnel. The calculation of H_c^* and D_c^* are given in Eq. (19) and Eq. (20).

$$H_c^* = \frac{H_c}{H_i} \quad (19)$$

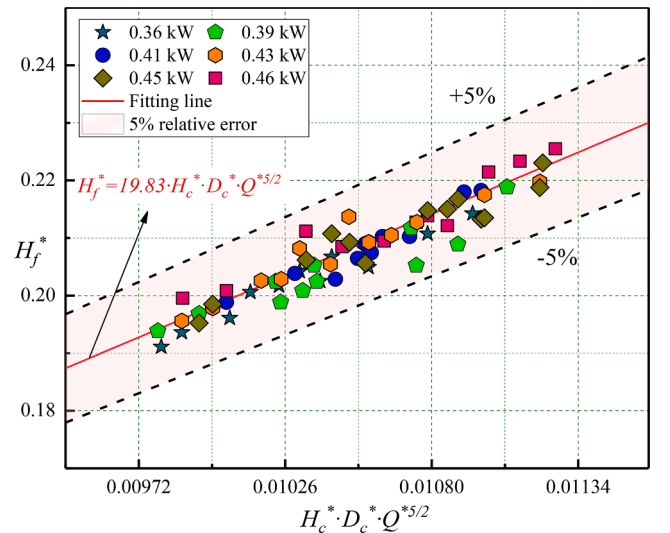


Fig. 19. Relationship between dimensionless flame height with dimensionless HRR.

$$D_c^* = \frac{D_c}{D/2} \quad (20)$$

Fig. 19 shows the relationship of the dimensionless H_f^* with Q^* , H_c^* and D_c^* , and a well linear trend could be found between them. The γ could be quantized by H_c^* and D_c^* and Eq. (18) can be expressed as follows:

$$\gamma = k \cdot H_c^* \cdot D_c^* \quad (21)$$

By fitting the experimental data, it can be determined that $k = 19.83$. Eventually, with the consideration of H_c^* and D_c^* , the dimensionless flame extension height of a free flame subject to cable fire in a utility tunnel can be expressed as follows:

$$H_f^* = 19.83 \cdot H_c^* \cdot D_c^* \cdot Q^{*5/2} \quad (22)$$

It can be found that convergence of fitted line with experimental data performs relatively well. The fitted line error is within 5 % of the experimental data in this study, with a correlation coefficient being 0.98. Additionally, as shown in Fig. 20, the prediction model can describe the data points in previous works (Zhang et al., 2014; Zavaleta and Hanouzet, 2019; An et al., 2020) with a relative error less 10 %. However, some of the results in An's experiments, under the fire scenario of multi-layer cable, are slightly higher than the predicted values. This is mainly due to the fact that once the layer spacing is small, the low layer cable could ignite the cables on the upper layer and rise the flame height. The data of Zavaleta's work are based on full-scale cable fire experiments. The dimensionless flame heights are remarkably close to the results proposed of prediction model in this paper. The deviation is due to the fact that the Zavaleta's experiments were conducted in an open space and the fire flame was not influenced by the tunnel ceiling and side wall. Thus, it is proved that Eq. (22) can be applied in the prediction of flame extension height in case the flame not touching the ceiling.

4.3. Flame spread characteristics

As Fig. 21 shows, when the vertical height of the cable fire from the ground is 30 cm, the flame spread velocity in the horizontal direction tends to increase as the HRR grows. Furthermore, the flame travels faster with an increasing transverse distance. The flame spread rate in the horizontal direction is 7.26 cm/s, at which the HRR is 0.46 kW and the near wall distance is 10 cm. It is primarily a result of the cable burning more vigorously as the HRR increases. Additionally, once the cable fire is close to the wall, the air inflow is restricted, inhibiting the fire spread

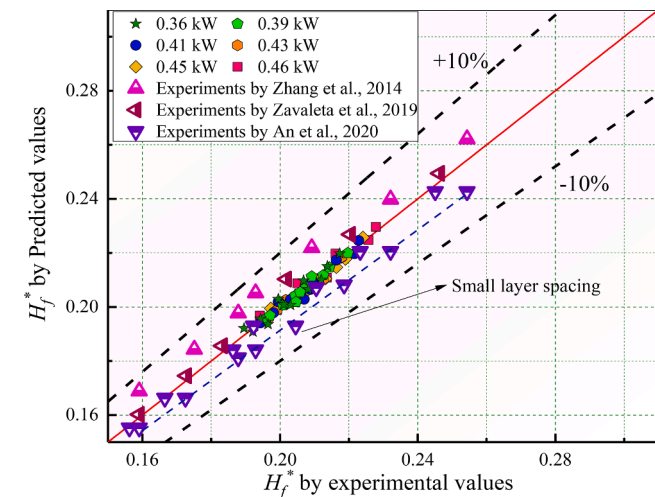


Fig. 20. Comparison of the dimensionless flame height among the predicted model, experimental results, and previous data.

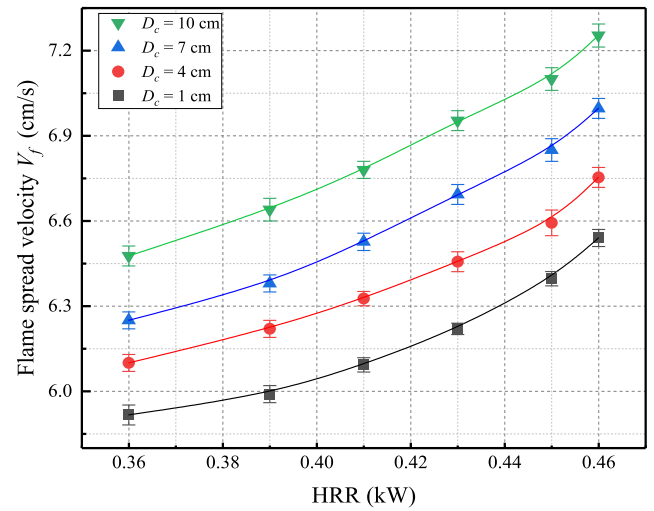


Fig. 21. Flame spread velocity with HRRs and transverse distance under 30 cm height.

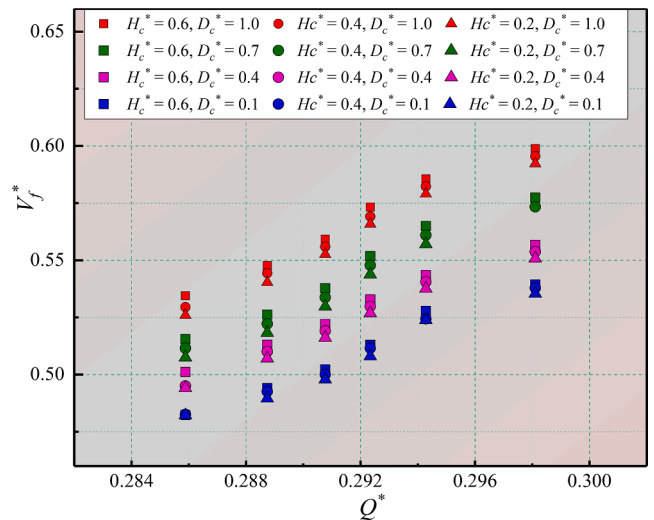


Fig. 22. Experimental results of dimensionless flame height against HRR.

in the horizontal direction. Fig. 22 illustrates the variation of the dimensionless flame spread rate V_f^* versus HRR. Note that the dimensionless spread rate shows a positive correlation increase with the dimensionless HRR. And the formula can be described as follows.

$$V_f^* \sim \eta \cdot Q^{*5/2} \quad (23)$$

where the η is a constant number; V_f^* is the dimensionless spread rate and it can be calculated as follows:

$$V_f^* = \frac{V_f}{\sqrt{gl}} \quad (24)$$

where l is the cable length.

More importantly, not only independent of the HRR of the cable, the H_c^* and the D_c^* also have significant effects on the V_f^* . This suggests that these factors should be further taken into account in the prediction model to be suitable for more complex scenarios. Thus, the η could be quantized by H_c^* and D_c^* and can be expressed as follows:

$$\eta = i \cdot H_c^* \cdot D_c^* \quad (25)$$

From the fitted results in Fig. 23, the coefficient number i can be determined as 51.46. The mean values of fitted line and the

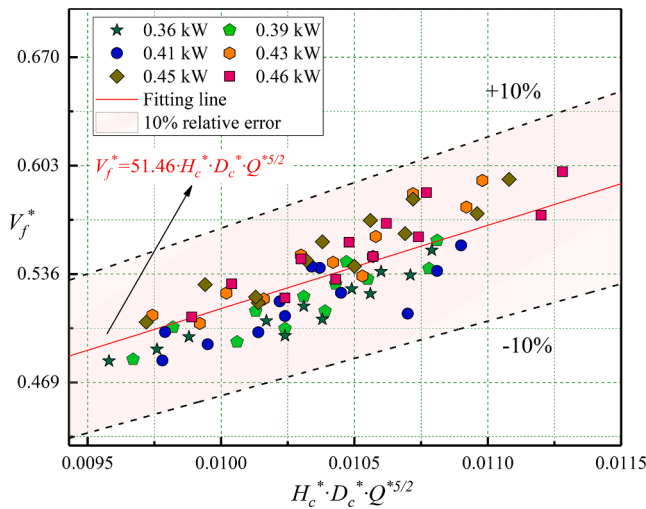


Fig. 23. Relationship of dimensionless flame height with dimensionless HRR.

experimental results achieve good agreements. And, the relationship between dimensionless flame spread rate and dimensionless Q^* , H_c^* and D_c^* can be obtained as the following:

$$V_f^* = 51.46 \cdot H_c^* \cdot D_c^* \cdot Q^{*5/2} \tag{26}$$

As clearly shown in Fig. 24, the comparison of the dimensionless flame spread rate predicted by Eq. (26) with experimental results in this work and other works (An et al., 2020; Zavaleta and Hanouzet, 2019). The predicted values are consistent with the experimental results and the error range between them is less than 10%. However, it should be noticed that the calculated values by Eq. (26) are smaller than some of the experimental results in An’s work. The difference can be illustrated as follows. An’s experiments were conducted under the fire scenario of multi-layer cable trays. Once the layer spacing is small, the low layer of the cable flame would ignite the cable on high layer. And it could cause a faster spread rate of the upper layer of cables. As the layer spacing exceeds the flame height, it is not possible to ignite the cable on upper layer. In this condition, the dimensionless flame spread rates are in good agreement with the predicted results. While the results of full-scale experiment, which conducted by Zavaleta with the arrangement of multiple cables on one layer tray, present a good agreement with the predicted results by Eq. (26). It sufficiently demonstrates that the prediction model proposed in this paper is applicable as an engineering

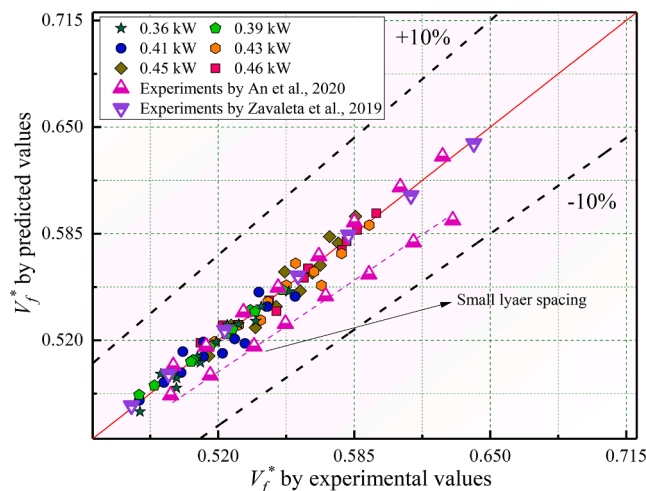


Fig. 24. Comparison of the dimensionless flame spread rate among predicted model with experimental results.

tool.

5. Conclusions

In this paper, an experimental investigation of the combustion and flame spread characteristics of cable fires in a utility tunnel of spontaneous combustion scenario was conducted. The results of the study reveal the following key findings:

1. The HRR of spontaneous combustion cables was found to have an increasing trend with an increase in cable diameter. In the scenario of the dual-fire development phase, the HRR of the cable fire reaches its maximum value at 250 s after ignition, indicating the highest risk of fire. A formula for determining the HRR of spontaneous combustion cables was proposed using the oxygen consumption method and validated through comparison with the mass loss method.
2. The flame height and area were observed to increase with an increase in HRR, vertical height, and transverse distance. It was found that a 27.9% increase in fire HRR causes 11.9% flame height growth and 34.7% flame area expanding. The dimensionless H_c^* and D_c^* were defined to characterize the effect of ceiling and sidewall on cable fire. And a comprehensive prediction model for the flame height of spontaneous combustion cables in utility tunnels was proposed. The model showed good agreements with the experimental data and previous studies, including the experiment results of multi-layer cable fire and full-scale utility fire.
3. The flame spread rate in the horizontal direction was found to increase with an increase in HRR, vertical height, and transverse distance. A dimensionless model was established to describe the relationship between the flame spread rate and these factors. The prediction data was validated by experimental results of multi-layer cable fire and full-scale utility fire with a relative error of less than 10%, demonstrating that the prediction model proposed in this paper is applicable as an engineering tool.

The results of this study are valuable for the optimization of fire safety design and the prevention of cable fires in utility tunnels. However, it should be noted that the results are only valid in the context of a single cable in on layer tray under spontaneous combustion scenario. The effects of cable type, multi-layer cable trays, and tunnel dimensions on combustion and flame characteristics of cable fires in utility tunnels should be considered in future studies. Additionally, the HRRs of the cables used in this study were relatively small scale, and further studies with high HRR and multi-layered cable bridges are needed to scale up the findings of this research.

In conclusion, this research provides a significant contribution to the field of cable fires in utility tunnels and their impact on the electric power supply in cities. It presents a comprehensive experimental study that provides valuable insights into the behaviour of cable fires in the spontaneous combustion scenario. It highlights the need for further research in this field to understand the fire behaviour of cable fires in more complex scenarios. The results of this study can aid in the development of fire safety measures and prevent cable fires in utility tunnels, thereby improving the reliability and stability of the electric power supply in cities.

CRedit authorship contribution statement

Desheng Xu: Data curation, Investigation, Software, Methodology, Validation, Formal analysis, Writing – original draft. **Yanfeng Li:** Conceptualization, Formal analysis, Funding acquisition, Project administration, Resources, Software, Supervision, Writing – review & editing. **Jiaxin Li:** Supervision, Writing – review & editing. **Hua Zhong:** Writing – review & editing. **Junmei Li:** Methodology, Supervision. **Dengkai Tu:** Investigation. **Youbo Huang:** Writing – review & editing.

Declaration of Competing Interest

The authors declare that they have no known competing financial interests or personal relationships that could have appeared to influence the work reported in this paper.

Data availability

The data that has been used is confidential.

Appendix A. . Uncertainty analysis

The accuracy of test instruments is the key factor in the uncertainty of experimental results. Based on the root sum square (RSS), the uncertainty of calculation results can be well estimated (Kline and McClintock, 1953). By incorporating the uncertainty arising from each element, the calculation formula is expressed as the following:

$$\delta R = \left(\sum_{i=1}^N \left(\frac{\partial R}{\partial X_i} \delta X_i \right)^2 \right)^{1/2} \quad (\text{A1})$$

where δX_i is the contribution of each element's uncertainty; δR is the overall uncertainty.

(1) Uncertainty in the HRR measurement.

The HRR was measured using the oxygen consumption method as well as the mass loss method in this work. The uncertainty of measured HRR could be attributed to $\frac{\delta \dot{M}}{\dot{M}}$ and $\frac{\delta \dot{m}}{\dot{m}}$ can be obtained by the following equations:

$$\frac{\delta \dot{M}}{\dot{M}} = \pm \left[\left(\frac{\partial \dot{M}}{\partial \Delta M} \frac{\delta \Delta M}{\Delta M} \frac{\Delta M}{\dot{M}} \right)^2 + \left(\frac{\partial \dot{M}}{\partial \Delta t} \frac{\delta \Delta t}{\Delta t} \frac{\Delta t}{\dot{M}} \right)^2 + \left(\frac{\partial \dot{M}}{\partial A} \frac{\delta A}{A} \frac{A}{\dot{M}} \right)^2 \right]^{1/2} \quad (\text{A2})$$

$$\frac{\delta \dot{m}}{\dot{m}} = \pm \left[\left(\frac{\partial \dot{m}}{\partial \Delta m} \frac{\delta \Delta m}{\Delta m} \frac{\Delta m}{\dot{m}} \right)^2 + \left(\frac{\partial \dot{m}}{\partial \Delta t} \frac{\delta \Delta t}{\Delta t} \frac{\Delta t}{\dot{m}} \right)^2 + \left(\frac{\partial \dot{m}}{\partial A} \frac{\delta A}{A} \frac{A}{\dot{m}} \right)^2 \right]^{1/2} \quad (\text{A3})$$

where $\frac{\delta \Delta M}{\Delta M}$, $\frac{\delta \Delta m}{\Delta m}$, $\frac{\delta \Delta t}{\Delta t}$ and $\frac{\delta A}{A}$ respectively represent the relative uncertainties of the measured oxygen consumption, mass loss, time interval, and cable cross-section size. The uncertainty of oxygen concentration is mainly influenced by the accuracy of the gas analyser. And the uncertainty of mass loss measurement is primarily based on the precision of the weighing equipment. The relative error of all values has been described in detail in Section 3. Substituting these uncertainty values of test instruments into Eq. (A2) and Eq. (A3), the relative uncertainty of the measured HRR in this work is less than $\pm 5\%$.

(2) Uncertainty of the flame extension size measurement.

In this work, the temporal development of the cable fire was recorded by a digital camera and an image processing method was used to determine the flame extension size. The uncertainty of the flame extension length measurement is mainly determined by the optical distortion error, mechanical error, and electrical error of the digital camera. Based on the technical guide of these errors, the relative error of all values is determined as $\pm 2\text{ mm}$. The relative uncertainty of flame extension length is calculated as $\frac{\delta L}{L} = \pm \left(\frac{\pm 2 \text{ mm}}{L \text{ mm}} \right)$ and the maximum relative uncertainty is about $\pm 0.5\%$.

References

- An, W.G., Wang, T., Liang, K., Tang, Y.H., Wang, Z., 2020. Effects of interlayer distance and cable spacing on flame characteristics and fire hazard of multilayer cables in utility tunnel. *Case. Stud. Therm. Eng.* 22, 100784.
- Babrauskas, V., 1984. Development of the cone calorimeter—a bench-scale heat release rate apparatus based on oxygen consumption. *Fire. Mater.* 8 (2), 81–94.
- Babrauskas, V., Peacock, R.D., 1992. Heat release rate: The single most important variable in fire hazard. *Fire Saf. J.* 18, 255–272.
- Bai, Y.P., Zhou, R., Wu, J.S., 2020. Hazard identification and analysis of urban utility tunnels in China. *Tunn. Undergr. Space Technol* 106, 103584.
- Beji, T., Verstockt, S., Zavaleta, P., Merci, B., 2016. Flame spread monitoring and estimation of the heat release rate from a cable tray fire using video fire analysis (VFA). *Fire Technol.* 52, 611–621.
- Bertrand, R., Chaussard, M., Gonzalez, R., 2002. Behaviour of electrical cables under fire conditions. *Kemtechnik.* 67 (2–3), 116–120.
- Blevins, L.G., Pitts, W.M., 1999. Modeling of bare and aspirated thermocouples in compartment fires. *Fire Saf. J.* 33 (4), 239–259.
- Chow, W.K., Han, S.S., 2011. Heat release rate calculation in oxygen consumption calorimetry. *Appl. Therm. Eng.* 31 (2), 304–310.
- Delichatsios, M.M., Delichatsios, M.A., 1994. Upward flame spread and critical conditions for PE/PVC cables in a tray configuration. *Fire Saf. Sci.* 4, 433–444.
- Fan, C.G., Ji, J., Gao, Z.H., Sun, J.H., 2013. Experimental study on transverse smoke temperature distribution in road tunnel fires. *Tunn. Undergr. Space Technol.* 37 (6), 89–95.
- Gao, Z., Jie, J., Wan, H., Zhu, J., Sun, J., 2017. Experimental investigation on transverse ceiling flame length and temperature distribution of sidewall confined tunnel fire. *Fire Saf. J.* 91, 371–379.
- Gao, Z.H., Wan, H.X., Ji, J., Bi, Y.B., 2019. Experimental prediction on the performance and propagation of ceiling jets under the influence of wall confinement. *Energy* 178, 378–385.
- Grayson, S. J., Hees, P. V., Green, A. M., et al., 2000. Fire performance of electric cables—new test methods and measurement techniques. Final Report on the European Commission SMT Programme Sponsored Research Project SMT4-CT96-2059. 410(2), 49–60.
- Guo, F.Y., Ding, L., Gao, Z.H., Yu, L.X., Ji, J., 2020. Effects of wind flow and sidewall restriction on the geometric characteristics of propane diffusion flames in tunnels. *Energy* 198, 117332.
- He, K., Cheng, X.D., Li, Y.Z., Ingason, H., Shi, Z.C., Yang, H., Zhang, H.P., 2021. Experimental study on flame characteristics of double fires in a naturally ventilated tunnel: flame merging, flame tilt angle and flame height. *Tunn. Undergr. Space Technol.* 114, 103912.
- Hermouet, F., Rogaume, T., Guillaume, E., Richard, F., Marquis, D., Ponticq, X., 2021. Experimental characterization of the reaction-to-fire of an Acrylonitrile-Butadiene-Styrene (ABS) material using controlled atmosphere cone calorimeter. *Fire Saf. J.* 121, 103291.
- Hu, L.H., Lu, K.H., Delichatsios, M., He, L.H., Tang, F., 2012. An experimental investigation and statistical characterization of intermittent flame ejecting behavior of enclosure fires with an opening. *Combust. Flame.* 159 (3), 1178–1184.
- Hu, L.H., Wu, L., Liu, S., 2013. Flame length elongation behavior of medium hydrocarbon pool fires in cross air flow. *Fuel.* 111, 613–620.
- Hu, L.H., Sun, X.P., Zhang, X.L., Ren, F., 2019. Facade flame height and horizontal extending distance from opening of compartment fire with external sidewall wind. *P. Combust Inst.* 37 (3), 3859–3867.

- Huang, X.J., W, Y.H., R, Z.Y., Li, Z.B., Cheng, C.H., Chow, W.K., 2021. Experimental investigation on maximum ceiling jet temperature generated by a vertically spreading cable fire. *Fire Saf. J.* 120, 103125.
- Huang, P., Ye, S.L., Qin, L., Huang, Y.H., Yang, J., Yu, L.X., Wu, D.J., 2022. Experimental study on the maximum excess ceiling gas temperature generated by horizontal cable tray fires in urban utility tunnels. *Int. J. Therm. Sci.* 172, 107341.
- Huang, X.J., Zhu, H., Peng, L., Zheng, Z.H., Chow, W.K., 2019. Thermal characteristics of vertically spreading cable fires in confined compartments. *Fire Technol.* 55, 1849–1875.
- ISO Standard 5660-1, 1993. The International Organization for Standardization. Geneva.
- Janssens, M.L., 1991. Measuring Rate of Heat Release by Oxygen Consumption. *Fire Technol.* 27 (3), 234–249.
- Klauck, M., Nobrega, G., Reinecke, E.A., Bentaib, A., Maas, L., Chaumeix, N., Allelein, H. J., 2022. Experimental investigation on the impact of cable fire products from flame-retardant cables on catalysts used in passive auto-catalytic recombiners. *Prog. Nucl. Energy.* 152, 104365.
- Klein, R.A., 1997. "SFPE handbook of fire protection engineering (1995)." *Fire Saf. J.* 29 (1), 61–63.
- Kline, S.J., McClintock, F.A., 1953. Describing Uncertainties in Single-Sample Experiments. *Mechanical engineering (New York, N.Y.: 1919)* 75.
- Li, J.X., Li, Y.F., Li, J.M., Zhong, H., Zhao, J.L., Xu, D.S., 2023. Experimental analysis of the effect of the ramp slopes on the maximum exceedance temperature in a branched tunnel fire. *Tunn. Undergr. Space Technol.* 131, 104829.
- Martinka, J., Rantuch, P., Sulová, J., Martinka, F., 2018. Assessing the fire risk of electrical cables using a cone calorimeter. *J. Therm. Anal. Calorim.* 135 (6), 3069–3083.
- Meinier, R., Sonnier, R., Zavaleta, P., Suard, S., Ferry, L., 2018. Fire behavior of halogen-free flame retardant electrical cables with the cone calorimeter. *J. Hazard. Mater.* 342, 306–316.
- Otsu, N.A., 2007. Threshold Selection Method from Gray-Level Histograms. *Ieee. T. Syst. Man. Cy-s.* 9 (1), 62–66.
- Pan, R.L., Zhu, G.Q., Liang, Z.H., Zhang, G.W., Liu, H.N., Zhou, X., 2020. Experimental study on the fire shape and maximum temperature beneath ceiling centerline in utility tunnel under the effect of curved sidewall. *Tunn. Undergr. Space Technol.* 99, 103304.
- Pan, R.L., Zhu, G.Q., Xu, G., Liu, X., 2022. Experimental and theoretical analysis on extension flame length of buoyancy-induced fire plume beneath the curved ceiling. *Tunn. Undergr. Space Technol.* 122, 104365.
- Passalacqua, R., Cortes, P., Taylor, N., Beltran, D., Zavaleta, P., Charbaut, S., 2013. Experimental characterisation of iter electric cables in postulated fire scenarios. *Fusion. Eng. Des.* 88 (9–10), 2650–2654.
- Poreh, M., Garrad, G., 2000. A study of wall and corner fire plumes. *Fire Saf. J.* 34, 81–98.
- Standard, I.E.C., 1994. Thermocouples, Part I: reference tables. IEC Publication 584–1. Intl. Electrotech. Com.
- Tang, F., Hu, P., He, Q., Zhang, J., Wen, J., 2021. Effect of sidewall on the flame extension characteristics beneath a ceiling induced by carriage fire in a channel. *Combust. Flame.* 223, 202–215.
- Tao, C.F., He, Y.Y., Zhuang, Y., Qian, Y.J., Cheng, X.Z., Wang, X.S., 2017. The investigation of flame length of buoyancy-controlled gas fire bounded by wall and ceiling. *Appl. Therm. Eng.* 127, 1172–1183.
- Tao, H.W., Zhang, X.C., Guo, Z.M., Zeng, W.Y., Huang, X.J., Zheng, Z.H., Xu, W.B., 2019. Combustion characteristics and heat release rate of vertical cable fire for sustainable energy system in an analogue underground compartment. *Sustain. Cities. Soc.* 45, 406–412.
- Tewarson, A., Khan, M.M., 1989. Flame propagation for polymers in cylindrical configuration and vertical orientation. *Symp. (Int.) Combust.* 22 (1), 1231–1240.
- Vandecasteele, F., Merci, B., Verstockt, S., 2016. Reasoning on multi-sensor geographic smoke spread data for fire development and risk analysis. *Fire Saf. J.* 86, 65–74.
- Wang, T.Y., Tan, L.X., Xie, S.Y., Ma, B.S., 2018. Development and applications of common utility tunnels in China. *Tunn. Undergr. Space Technol.* 76, 92–106.
- Ye, K., Tang, X., Zheng, Y., Ju, X., Peng, Y., Liu, H., Wang, D., Cao, B., Yang, L., 2021. Estimating the two-dimensional thermal environment generated by strong fire plumes in an urban utility tunnel. *Process Saf. Environ. Prot.* 148, 737–750.
- Zavaleta, P., Hanouzet, R., 2019. Improved assessment of fire spread over horizontal cable trays supported by video fire analysis. *Fire Technol.* 55, 233–255.
- Zhang, Y.L., Chen, C.K., Lei, P., Wang, Z.Y., Jiao, W.B., 2021a. Experimental investigation on ceiling flame extension subject to relative large area of liquid fuel in a channel-like structure with confined portals. *Tunn. Undergr. Space Technol.* 112, 103899.
- Zhang, X.C., Hu, L.H., Zhu, W., Zhang, X.L., Yang, L.Z., 2014. Flame extension length and temperature profile in thermal impinging flow of buoyant round jet upon a horizontal plate. *Appl. Therm. Eng.* 73, 15–22.
- Zhang, X., Hu, L., Zhang, X., 2021b. Flame lengths in two directions underneath a ceiling induced by line-source fire: An experimental study and global model. *Proc. Combust. Inst.* 38 (3), 4561–4568.
- Zhang, X.C., Tao, H.W., Xu, W.B., Liu, X.Z., Li, X.D., Zhang, X.L., Hu, L.H., 2017. Flame extension lengths beneath an inclined ceiling induced by rectangular-source fires[J]. *Combust. Flame.* 176, 349–357.
- Zhou, T., Zhou, Y., Fan, C., Wang, J., 2020. Experimental study on temperature distribution beneath an arced tunnel ceiling with various fire locations. *Tunn. Undergr. Space Technol.* 98, 103344.